© 2015. Published by The Company of Biologists Ltd | Journal of Experimental Biology (2015) 218, 3295-3307 doi:10.1242/jeb.122408

RESEARCH ARTICLE

Body appendages fine-tune posture and moments in freely manoeuvring fruit flies

Ruben Berthé and Fritz-Olaf Lehmann*

ABSTRACT

The precise control of body posture by turning moments is key to elevated locomotor performance in flying animals. Although elevated moments for body stabilization are typically produced by wing aerodynamics, animals also steer using drag on body appendages, shifting their centre of body mass, and changing moments of inertia caused by active alterations in body shape. To estimate the instantaneous contribution of each of these components for posture control in an insect, we three-dimensionally reconstructed body posture and movements of body appendages in freely manoeuvring fruit flies (*Drosophila melanogaster*) by high-speed video and experimentally scored drag coefficients of legs and body trunk at low Reynolds number. The results show that the sum of leg- and abdomen-induced yaw moments dominates wing-induced moments during 17% of total flight time but is, on average, 7.2-times (roll, 3.4-times) smaller during manoeuvring. Our data reject a previous hypothesis on synergistic moment support, indicating that drag on body appendages and mass-shift inhibit rather than support turning moments produced by the wings. Numerical modelling further shows that hind leg extension alters the moments of inertia around the three main body axes of the animal by not more than 6% during manoeuvring, which is significantly less than previously reported for other insects. In sum, yaw, pitch and roll steering by body appendages probably fine-tune turning behaviour and body posture, without providing a significant advantage for posture stability and moment support. Motion control of appendages might thus be part of the insect's trimming reflexes, which reduce imbalances in moment generation caused by unilateral wing damage and abnormal asymmetries of the flight apparatus.

KEY WORDS: Aerodynamics, Body appendages, *Drosophila*, Free flight, Insect flight, Locomotion, Moment control, Moments of inertia, Posture stability

INTRODUCTION

Locomotion during migration, territory defence, routine commuting, foraging and escape behaviour is vital to the reproductive effectiveness and survival of many animals (Alexander, 2003). A critical task during locomotion is the control of body posture, which is tightly linked to the production and control of locomotor forces for propulsion and the corresponding moments for turning control (Ellington, 1984a,b). While locomotion involving contact with solid ground benefits from static stability, flying animals achieve body stability and thus flight path control with the help of aerodynamic friction of their environment. Active manoeuvring and directed aerial descent such as gliding thus depend on the animal's ability to fine-tune the benefits of three distinct, major physical mechanisms for posture control: aerodynamic lift and drag on wings and body (Pennycuick, 1968, 1971), active control of the centre of body mass and thus distance to aerodynamic force vectors (Cook and Spottiswoode, 2006; Ellington, 1984a), and modifications of the body's moments of inertia by active changes in body shape (Libby et al., 2012).

The control of moments of inertia is highly effective even in terrestrial animals, for example, during falling and jumping, in which rats maintain an upright body posture by twisting their entire body (Laouris et al., 1990) and geckos and lizards by beating their heavy tails (Jusufi et al., 2008; Libby et al., 2012). In preparation for targeted jumps, moreover, flightless mantis generate a controlled whole-body spin by adjustment of their centre of mass (Burrows et al., 2015). Since active modification in body shape leads to a change in moments of inertia, this mechanism also enables astronauts to control their body orientation without air friction (Kane and Scher, 1970; Kulwicki et al., 1962). By contrast, gliding and actively flying animals typically control moments and posture by alterations in the lift and drag characteristics of the wings (Ellington, 1984a,c, 1991). Although wing aerodynamics predominantly determine moments for posture control, an increasing number of studies suggest that aerial steering is effectively supported by the aerodynamics of body appendages such as the legs and abdomen. Arboreal ants and other wingless, gliding hexapods, for example, effectively control their aerial descent from tree to tree by steering with their hind legs (Yanoviak et al., 2010) and lateral cerci, respectively (Yanoviak et al., 2009). If the hind legs are cut, the tree trunk landing success is severely attenuated between 35 and 60%. Leg steering is also of great importance for drag control in birds. Depending on body posture, pigeons and griffon vultures, for example, may increase their total body drag coefficients during forward flight by factors of approximately 2 and 3, respectively, depending on the extension of their feet (Pennycuick, 1968, 1971). As a consequence, feet adduction in birds during smooth weather conditions leads to an increase in gliding distance whereas during manoeuvres, the feet appear (Pennycuick, 1960).

The vast majority of previous studies on the significance of body appendages for force and moment support in actively flying animals were conducted in insects such as the small fruit fly (Götz et al., 1979; Zanker, 1988b), the house fly (Zanker et al., 1991), orchid bees (Combes and Dudley, 2009) and moths (Cheng et al., 2011; Hedrick and Daniel, 2006). Early studies on various freely flying insect species suggested that leg steering and shifting the insect's centre of body mass support wing-induced moments during manoeuvring (Ellington, 1984d). This hypothesis was further investigated under visual stimulation mimicking yaw turns, during which tethered flying flies bend hind legs and abdomen in the horizontal to the inner side of the intended turn (Götz et al., 1979; Zanker, 1988a,b; Zanker et al, 1991). Visual stimulation mimicking body pitching, by contrast, leads to bending of the abdomen in the vertical, with upward bending during upward motion of the visual pattern (Dyhr et al., 2013; Frye, 2001;

Department of Animal Physiology, University of Rostock, 18059 Rostock, Germany.

*Author for correspondence (fritz.lehmann@uni-rostock.de)

Received 17 March 2015; Accepted 21 August 2015

Journal of Experimental Biology (2015) 218, 3295-3307 doi:10.1242/jeb.122408

Hinterwirth and Daniel, 2010). Mathematical models of the latter behaviour demonstrate that abdominal steering is, at least to some extent, sufficient to maintain body posture in the hawkmoth (Cheng et al., 2011; Dyhr et al., 2013; Hedrick and Daniel, 2006). Besides vision, some insects such as desert locusts also bend their abdomen in response to changing air flow conditions (Arbas, 1986). It has been suggested that this behaviour mimics an aerodynamic rudder that helps the animal to orient into the direction of wind during flight (Camhi, 1970a,b).

Here, we show the significance of leg and abdominal steering on moments and body posture in freely manoeuvring fruit flies, estimating instantaneous moments due to wing motion, hind leg position and abdomen posture around the yaw, pitch and roll body axes, respectively. For this investigation, we: (1) used high-speed video to three-dimensionally reconstruct the body posture and extension angles of the legs and abdomen during various flight manoeuvres, (2) measured drag coefficients of hind legs and the body trunk in a wind tunnel and (3) derived turning moments from a numerical approach. In contrast to previous hypotheses, our data suggest that body appendages mostly attenuate rather than enhance wing-flapping-induced moments. We argue, moreover, that because of their small contribution to total moments, leg- and abdomen-induced moments should be considered as control systems for fine control, rather than systems that significantly enhance the production of moments during extreme flight manoeuvres.

RESULTS

Steering by wings and body appendages

Our recorded flight sequences cover various flight manoeuvres of female *Drosophila melanogaster* fruit flies, including rectilinear horizontal flight, ascending and descending flight, shallow turns and rapid flight saccades, in which animals rotate with angular peak velocity of up to 1074 deg s^{-1} (mean, 504±49.1 deg s^{-1}, *N*=6 saccades) around the vertical yaw axis (Fig. 1A,B). The mean of all data points within each flight sequence that fell within the top 1% maximum of horizontal (vertical) velocity values was 0.26±0.13 m s^{-1} (0.15±0.11 m s^{-1}) while the mean of all data samples amounts to 0.21±0.12 m s^{-1} (0.11±0.11 m s^{-1}, *N*=81 flight sequences). The free flight analysis highlights that body yaw, pitch and roll angles continuously change during manoeuvring flight, exhibiting small changes of several degrees during straight flight and pronounced changes in body posture of up to ∼30 deg roll angle during rapid turns (Fig. 1A,C). The normalized histograms of posture angles demonstrate a mean body pitch of ∼30.6±9.7 deg and a mean roll angle near zero of −0.6±9.4 deg (*N*=24,579 video frames) during flight.

Free flight manoeuvres in *Drosophila* are accompanied by extensive movements of hind legs and the abdomen. On average, the animals bend their abdomen vertically downward by ∼10.1±5.3 deg with respect to the longitudinal body axis at a mean horizontal deflection angle of the abdomen close to zero (2.0±3.5 deg). Abdomen steering angles typically vary ±15 deg around its mean value (Fig. 1D). By contrast, leg extension angles (right−left) vary between −35 and 35 deg, with mean vertical and horizontal leg extension angles of 108±15.1 deg and 112±13.7 deg, respectively (Fig. 1E,F). For a definition of angles refer to the Materials and methods.

To evaluate the contribution of moments caused by changes in aerodynamic drag on both body trunk (head, thorax, abdomen, fore and middle legs) and hind legs to wing flapping-induced moments during flight manoeuvres, we systematically analysed the magnitude and coherence of the three components for total moment control (Fig. 2B,C). Fig. 2 shows the moment

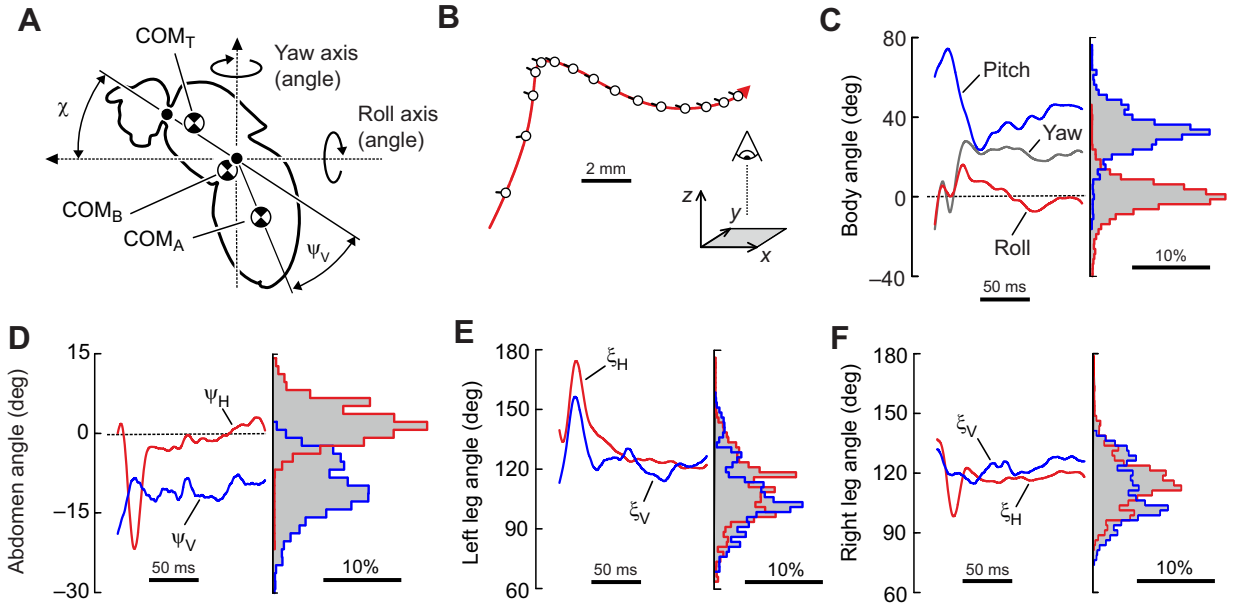

Fig. 1. Body posture, hind leg extension and abdomen bending in freely manoeuvring fruit flies. (A) Yaw, pitch and roll angles and corresponding axes. The three-dimensional, instantaneous position of the centre of body mass COM_B was reconstructed from the centre of abdominal mass COM_A and the centre of the combined mass of thorax, head and legs COM_T. ψ_V, deflection angle of the abdomen in the vertical; χ, body pitch angle. (B) Top view (*x*–*y* plane) on a flight path of a single fly cruising freely. Open dots indicate the centre of body mass every 10 ms, i.e. equal to every 35th recorded video frame and attached lines show the orientation of the animal's longitudinal body axis. (C) Yaw, pitch and roll angles plotted for the flight sequence shown in B. Yaw angles are scored with respect to the external coordinate system. Angles around the roll axis to the right (clockwise) and upward pitching are positive. (D–F) Abdominal deflection and leg extension angles in the vertical (ψ_V, ζ_V) and horizontal (ψ_H, ζ_H) for sequence in B, respectively. Normalized angle histograms of all flight sequences are shown on the right in respective colours. Data were derived from 7.03 s total flight time. *N*=81 flight sequences recorded in 14 flies.

Journal of Experimental Biology (2015) 218, 3295-3307 doi:10.1242/jeb.122408

components for yaw (Fig. 2E), pitch (Fig. 2F) and roll (Fig. 2G) of the flight manoeuvre in Fig. 2A. The data suggest that aerodynamic drag- and mass-shift-induced moments are only small fractions of total moments acting on the fly body (Fig. 2D–G). We derived the total moments from the changes in body posture and a numerical framework (cf. Materials and methods). The top 1% maximum, absolute total moment of all data around the yaw, pitch and roll axes was 11.2, 10.2 and 26.8 nN m, respectively (N=246 samples). On average, the individual contributions of hind-leg-induced moments were ~41.3- (yaw), 11.2- (roll) and 78.3-times (pitch), and contributions of the body trunk ~7.9- (yaw) and 3.8-times (pitch) smaller than total moments produced by wings, hind legs, and trunk (Table 1). Further calculations of moments using static, non-moveable legs and abdomen with average posture (M_I=0, ζ_V=105 deg, ζ_H=143 deg, ψ_V=0 deg, ψ_H=0 deg) show that 'static' absolute M_D* differs by ~3.4 pN m (46%, yaw), 16.7 pN m (47%, pitch), and 3.7 pN m (21%, roll) from M_D produced by moving legs and abdomen (single animal, Fig. 3). Considering only static legs (abdomen), mean M_D* differs by ~10.0±9.5 pN m (6.4±8.7 pN m, yaw), 19.4±18.9 pN m (29.8±21.2 pN m, pitch) and 15.0±14.9 pN m (7.1±8.0 pN m, roll) from M_D (N=81 flight sequences).

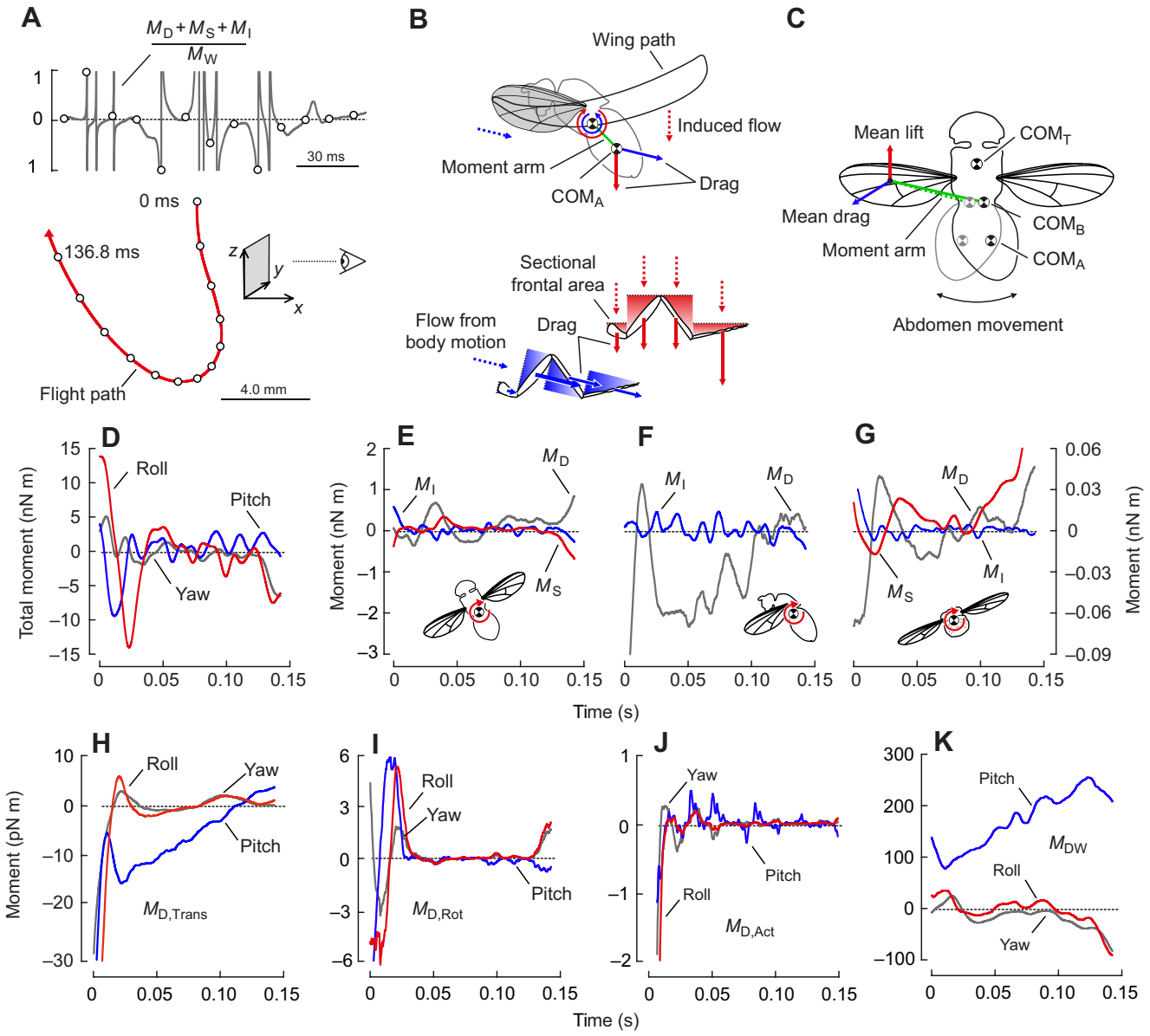

Fig. 2. Instantaneous moments of a fruit fly flying freely inside a random dot flight arena. (A) Side view (y–z plane) of a flight path with superimposed body positions (open dot) plotted every 11.4 ms during the 142 ms sequence. Time trace shows the ratio between the sum of body-appendage-induced (numerator) and wing-flapping-induced moments (denominator). Data are clipped at ±1. (B) Draft illustrating moments induced by aerodynamic forces acting on the fly. (C) Draft illustrating moments due to body mass shift. (D) Total moment around the fly's centre of mass (COM_B) for sequence shown in A. (E) Yaw, (F) pitch and (G) roll moments around COM_B. Positive values indicate clockwise moments around yaw, pitch and roll axes (cf. Fig. 1A). Body drag-induced moment (M_D, right axis) results from aerodynamic drag on abdomen and hind legs, while inertia-induced moment (M_I, left axis) is estimated from relative movements of abdomen and hind legs. Mass shift-induced moment (M_S, left axis) is the product of stroke cycle-averaged aerodynamic force of each wing and the moment arm between the wing's centre of force at mid-downstroke and COM_B. (H) Fractions of drag-induced moment due to body translation $M_{D,Trans}$, (I) body rotation $M_{D,Rot}$ and (J) self-induced moments due to active movement of abdomen and hind legs ('paddling') relative to thorax $M_{D,Act}$. (K) Moment induced by the wings' mean downwash (induced flow) M_{DW}. M_{DW} is not considered for total M_D in E–G. See text and legend of Table 1 for more information.

Journal of Experimental Biology

Journal of Experimental Biology (2015) 218, 3295-3307 doi:10.1242/jeb.122408

Table 1. Mean and maximum turning moments in freely manoeuvring fruit flies

Moment	Axis	Mean performance	Maximum performance
M_M (nN m)	Yaw	1.65±1.00	6.29±3.18 (11.2)
	Pitch	2.23±0.81	7.68±2.73 (10.2)
	Roll	3.13±3.41	9.63±8.92 (26.8)
M_D (nN m)	Yaw	0.03±0.03	0.06±0.05 (0.16)
	Pitch	0.10±0.08	0.16±0.10 (0.36)
	Roll	0.04±0.04	0.07±0.06 (0.22)
M_S (nN m)	Yaw	0.21±0.39	0.46±0.62 (2.55)
	Roll	0.83±0.72	1.52±0.98 (3.81)
M_I (nN m)	Yaw	0.16±0.05	0.82±0.41 (0.96)
	Pitch	0.34±0.10	1.52±0.65 (1.84)
	Roll	0.15±0.08	0.84±0.68 (1.29)
$M_{D,Leg}$ (pN m)	Yaw	35.2±30.9	63.5±52.1 (171)
	Pitch	106±85.9	159±98.4 (386)
	Roll	41.2±39.2	74.0±58.7 (220)
$M_{D,Abd}$ (pN m)	Yaw	5.72±5.92	14.7±12.9 (39.7)
	Pitch	13.6±11.2	31.0±19.5 (68.6)
	Roll	4.73±5.56	13.8±14.5 (40.8)
$M_{D,Trans}$ (pN m)	Yaw	19.6±22.8	36.1±40.5 (133)
	Pitch	47.0±54.8	78.9±86.9 (324)
	Roll	16.9±22.5	31.2±38.2 (150)
$M_{D,Rot}$ (pN m)	Yaw	0.39±0.93	1.92±3.58 (9.38)
	Pitch	0.39±0.73	1.89±3.34 (8.30)
	Roll	0.55±1.68	2.72±7.14 (16.3)
$M_{D,Act}$ (pN m)	Yaw	0.05±0.14	0.57±1.88 (1.45)
	Pitch	0.09±0.15	0.92±2.44 (2.18)
	Roll	0.04±0.08	0.44±1.28 (1.92)

Data are absolute values, ignoring sign and thus direction of moments. Mean performance±s.d. was calculated from 81 flight sequences and maximum performance±s.d. from means of the 1% largest values of each flight sequence. Value in parentheses is the mean of the 1% largest values of all sequences (N=24,596 data samples). M_M, total moment derived from body motion; M_D, sum of moments induced by drag on body trunk and hind legs; M_S, moment induced by displacement of the fly's centre of body mass; M_I, moment due to inertia of hind legs and abdomen; $M_{D,Leg}$, moment induced by drag on hind legs; $M_{D,Abd}$, moment induced by drag on abdomen; $M_{D,Trans}$, drag-induced total moment due to translational body motion; $M_{D,Rot}$, drag-induced total moment due to rotational body motion; $M_{D,Act}$, drag-induced moment due to active movements of abdomen and hind legs relative to fly thorax.

The magnitude of turning moments depends on the product of moment arm and aerodynamic force, and thus on local air velocities on the legs and abdomen. These velocities result from three distinct kinematic components: the body's translational motion (for-, up- and sideward), its rotational motion around the three main body axes, and active leg motion relative to the body (Fig. 1A, Table 1). For completeness, we also considered the wing's induced flow (downwash) on legs and body, which is outlined in more detail in a section below. The moments around the fly's main axes (yaw, pitch, roll) due to translational body motion are shown in Fig. 2H, rotational motion is shown in Fig. 2I, active leg motion in Fig. 2J, and moments due to induced flow from the beating wings in Fig. 2K. The data suggest that body translation predominately determines moment control in fruit flies cruising at mean forward speed of 253±137 mm s^{-1}, while the contribution of rotational body motion is small owing to small angular speeds and a decreasing velocity gradient from leg tip to base (Table 1). Mean tarsal velocity of the hind legs due to body rotation amounts to only ~13.4±14.7 mm s^{-1} and the 1% maximum does not exceed 107 mm s^{-1}. The velocity component due to active leg motion (7.04±7.99 mm s^{-1}) is almost negligible and 36- and 2-times smaller than the velocities induced by body translation and rotation, respectively. We obtained similar results for active translation motion of the abdomen (3.77±1.64 mm s^{-1}) that compares to a mean body rotation-induced velocity of 6.75±4.60 mm s^{-1}.

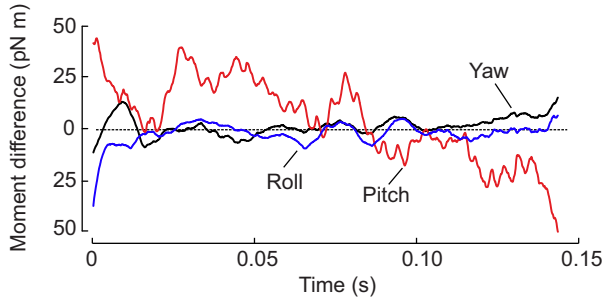

Fig. 3. Difference of instantaneous drag-induced moments M_D minus M_D* around COM_B. Moments (M_D*) for yaw (black), pitch (red) and roll (blue) were calculated assuming static, non-moveable hind legs and abdomen, for the example shown in Fig. 2. The difference highlights the contribution of active leg and abdomen movements during manoeuvring flight. See text for more details.

Although our data indicate that drag-based steering by hind legs is likely to be 7.6-fold more effective than drag-based steering by the abdomen, the significance of body appendages for moment control during manoeuvring flight is limited (Fig. 4A,B). An analysis on the relative contribution of drag-, mass shift- and inertia-induced moments for yaw control shows that the sum of all three moment components exceeds wing flapping-induced moments in only 16.8% (22.9% for roll) of total flight time (Fig. 4C,D). Drag-based moments alone are higher than wing flapping moments in 1.7% (yaw) and 0.9% (roll) of the flight time (Fig. 4E,F). In other words: during half of total flight time, the total moments produced by body appendages for yaw and roll amount to only 2.0% and 3.3% of wing-induced moments, respectively.

Coherence of steering moment components

In contrast to previous tethered flight studies on vision-induced yaw steering in *Drosophila*, hind leg and abdomen deflection is more variable in free flight. Our data even suggest that leg and abdomen deflection is broadly independent from total, wing flapping-dominated moment control. We found that only in 51.8% of total flight time, the sign of the instantaneous, relative (left−right), horizontal leg extension angle ζ_H (cf. Materials and methods) equals the sign of the total (sum of wing- and body-induced) yaw moment M_M. At these instants, the unsigned difference between left and right horizontal leg extension angle is 11.2 deg ±8.41 deg (mean, N=81 flight sequences). At times (48.2% flight time) at which relative leg extension angle and total yaw moment had a different sign, the unsigned difference between left and right ζ_H is 10.1 deg ±8.17 deg (mean, N=81 flight sequences). For an additional statistical test, we dichotomized the data with +1 (−1) that represents times at which leg extension and yaw moments had equal (opposite) direction. We found no significant difference between the two means for all flight sequences (0.03±0.35, Wilcoxon test, P=0.14, N=81). Statistical comparison of the relationship between yaw moments and horizontal abdomen bending yielded a similar result: times with equal sign occurred during 51.2% of the total time without a statistical difference from zero for the dichotomized data (0.02±0.34, Wilcoxon test, P=0.16, N=81).

To further investigate the relationship between the various sources of body moments, we conducted moment coherence and correlation analyses on yaw and roll (Figs 5 and 6). The moment coherence analysis suggests that the sign of wing-flapping- and

Journal of Experimental Biology

Journal of Experimental Biology (2015) 218, 3295-3307 doi:10.1242/jeb.122408

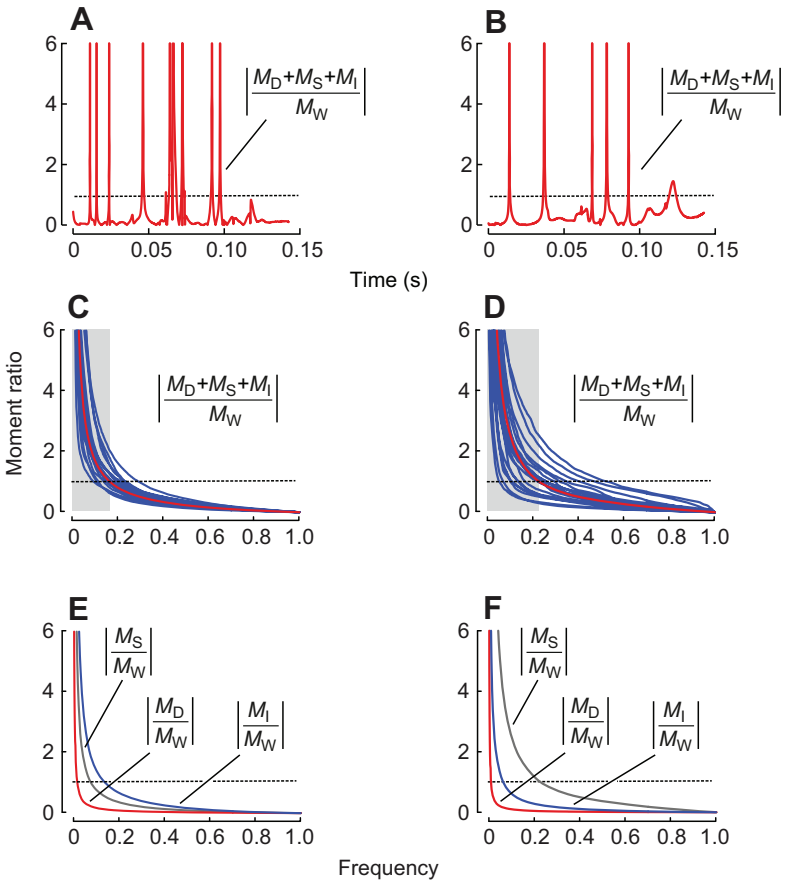

Fig. 4. Frequency of moment ratios during yaw and roll steering in fruit flies. (A,C,E) Yaw steering. (B,D,F) Roll steering. (A,B) Ratio between moments produced by body drag (M_D), mass shift (M_S), inertia (M_I) and active wing flapping (M_W). (C,D) Moment ratio of the 20 longest flight sequences (blue) with means in red (N=81 sequences). Unity (dotted) indicates similar contribution of active (wing-flapping-induced) and passive (abdomen- and leg-induced) moments to total response. Grey area highlights the relative time at which rotational steering is dominated by leg and abdominal control. (E,F) Mean moment ratio between drag- (red), mass-shift- (grey), inertia- (blue) and wing-flapping-induced moments, respectively (N=81 sequences).

body-drag-induced yaw moments is opposite during ~63% (yaw; Fig. 5A) and 65% (roll) of total flight time. This means that leg-based steering inhibits rather than supports turning moments produced by wing flapping. The result is also consistent with findings from a correlation analysis on the temporal relationship between wing-flapping- and body-drag-induced moments of each flight sequence. The latter analysis shows significant, negative correlation coefficients of −0.45±0.36 and −0.54±0.36 (Pearson tests, N=73 and 74 significant correlations with P<0.05) for yaw (Fig. 5D) and roll, respectively. Corresponding coherence and correlation values between wing-flapping- and mass-shift-induced yaw moments are shown in Fig. 5B,E and data for the relationship between wing-flapping- and inertia-induced yaw moments in Fig. 5C,F. For completeness, Fig. 6 shows the remaining dependencies between the four sources of moment production (M_W, M_D, M_S and M_I). For statistical evaluation of the data, we tested the presented mean correlation coefficients against zero. The test yielded no significant differences of coefficients calculated for M_W versus M_S (coefficient for roll, −0.01±0.48; Wilcoxon test, P>0.99, N=64) and M_W versus M_I (coefficient for roll, 0.12±0.49; Wilcoxon test, P=0.09, N=58), whereas all other correlation values for yaw and roll moments were significantly different to zero (Wilcoxon test, P<0.01, Figs 5 and 6).

The significance of induced flow

We next address the potential significance of the wing's downwash on moment control by the body trunk and hind legs. Since the wings, legs and abdomen are mechanically linked, and the distance between the wings' stroke plane and hind legs is small, we excluded downwash-induced moments from the analyses in Figs 2–6, including Table 1. This is reasonable because body lift production by wing flapping should decrease with increasing downwash-induced drag on the legs and abdomen. To maintain weight support under these conditions, the animal must moderately increase its total body lift production, which, in turn, balances the moments produced by downwash-induced drag. However, at least to some degree, the downwash from the wings dissipates after its acceleration at the stroke plane, losing kinetic energy and altering the efficacy of momentum transfer from the wings to body and hind legs. The downwash-induced moments thus depend on the distance between the wings and body appendages (legs, abdomen), which varies during manoeuvring flight. In the following section, we evaluated the potential contribution of downwash to moment balance by estimation of instantaneous downwash velocity derived from body mass, instantaneous vertical body motion and using actuator disc theory (see the Materials and methods).

We considered downwash at various strengths and compared the resulting moments for yaw, pitch and roll with our previous approach (Figs 2–4). Fig. 7A shows a time trace of downwash-induced yaw moments (grey) of the flight sequence in Fig. 2A. We subsequently added fractions of these downwash moments to total drag-induced yaw moments M_D, in steps of 10% (coloured traces in Fig. 7A, cf. M_D in Fig. 2E). To determine the maximum potential effect of downwash on M_D, we calculated means of the unsigned top 1% maximum values of all 81 flight sequences (pooled data set, N=24,596 measurements). These values are ~4.7- (yaw), 7.6- (pitch) and 5.3-times (roll) larger than the means in Table 1. The results are shown in Fig. 7B for yaw, in Fig. 7C for pitch and in Fig. 7D for roll moments. Depending on downwash-induced moment, yaw moments change by ~21% and have a local

Journal of Experimental Biology (2015) 218, 3295-3307 doi:10.1242/jeb.122408

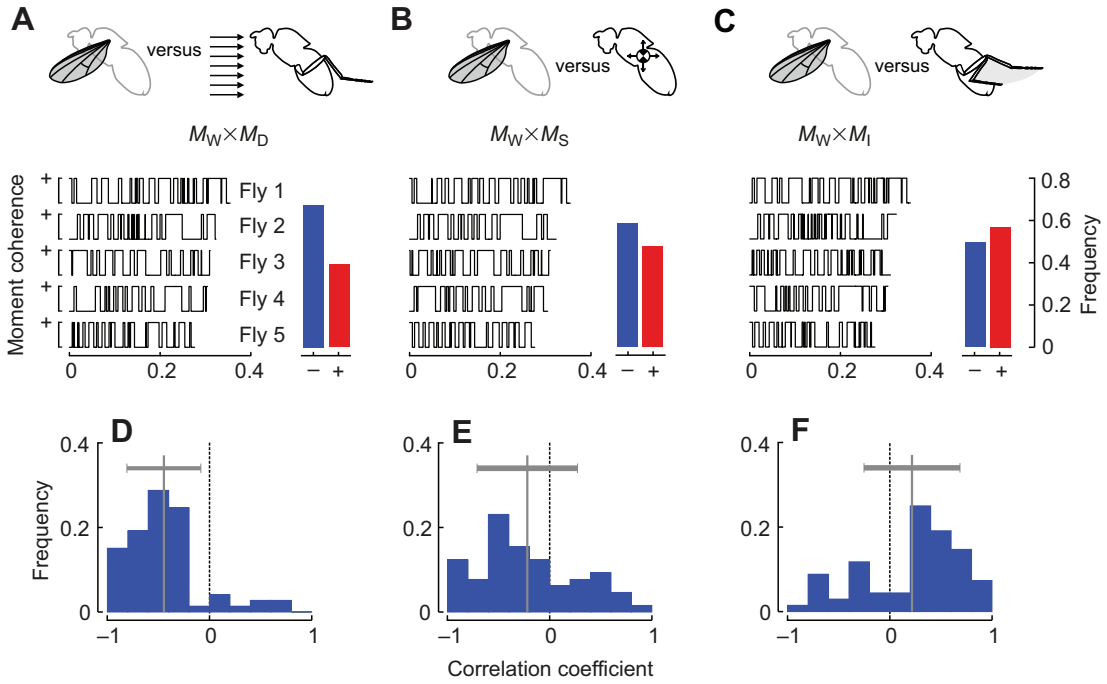

Fig. 5. Statistical analysis of coherence between the various components underlying yaw moment control. (A–C) Coherence of moments of the five longest recorded flight sequences (fly 1–5). Instantaneous coherence was scored as the product of moment sign between wing-flapping- and body-drag-induced moment in A, wing-flapping- and mass-shift-induced moments in B, and wing-flapping- and inertia-induced moments in C. Time-invariant relative frequency of coherence between the two instantaneous moments of all recorded data is shown on the right, respectively, with +(–) indicating equal (opposing) sign of moment. (D–F) Histogram of significant correlation coefficients (Pearson test, N=74 in D, N=64 in E, N=68 flight sequences in F) obtained from linear regression analysis between moments shown by the insets in A–C, respectively. A negative correlation coefficient suggests opposing direction of moments. Means±s.d.

minimum at 40% downwash. Pitch moments linearly increase with decreasing downwash by a factor of ~2.3, whereas roll moments appear to be widely independent of downwash-induced moments. Small effects were also obtained for the frequency of moment ratio M_D by M_W (yaw, Fig. 7E). Downwash-induced moments may also change the outcome of the correlation analysis. In two cases, the correlation coefficients decrease with increasing consideration of downwash-induced moments. This relationship is shown in

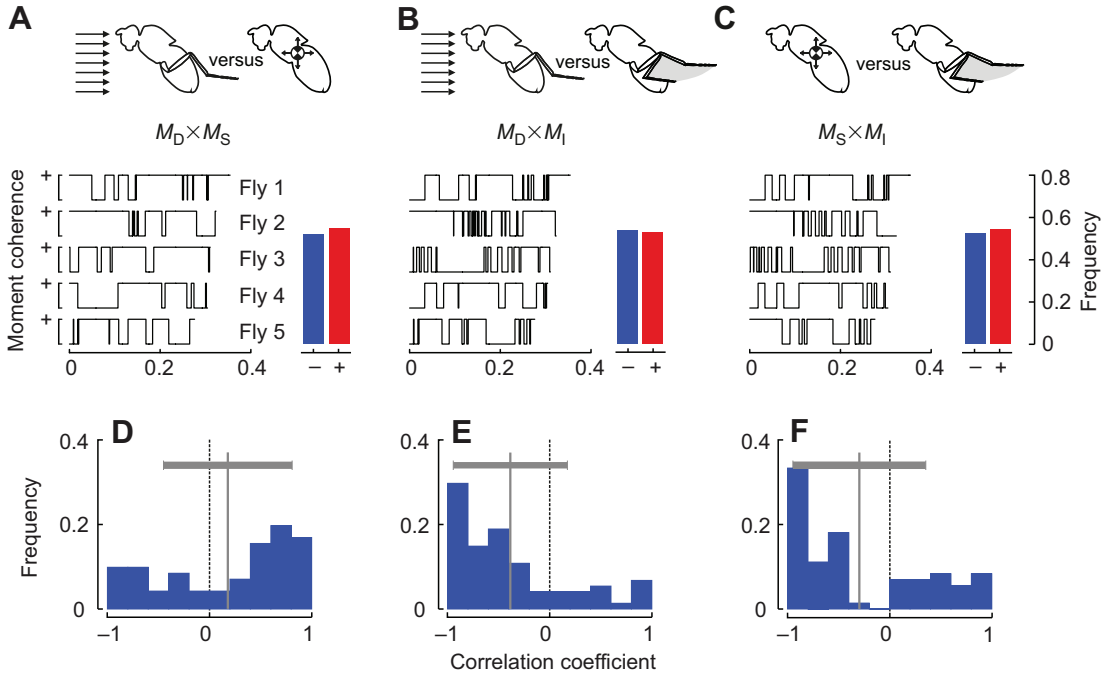

Fig. 6. Statistical analysis of coherence between the various components underlying yaw moment. (A–F) Coherence was scored as the product of moment sign between drag- and mass-shift-induced moment in A and D, drag- and inertia-induced moments in B and E, and mass-shift- and inertia-induced moments in C and F. See legend of Fig. 5 for a more detailed explanation.

Journal of Experimental Biology (2015) 218, 3295-3307 doi:10.1242/jeb.122408

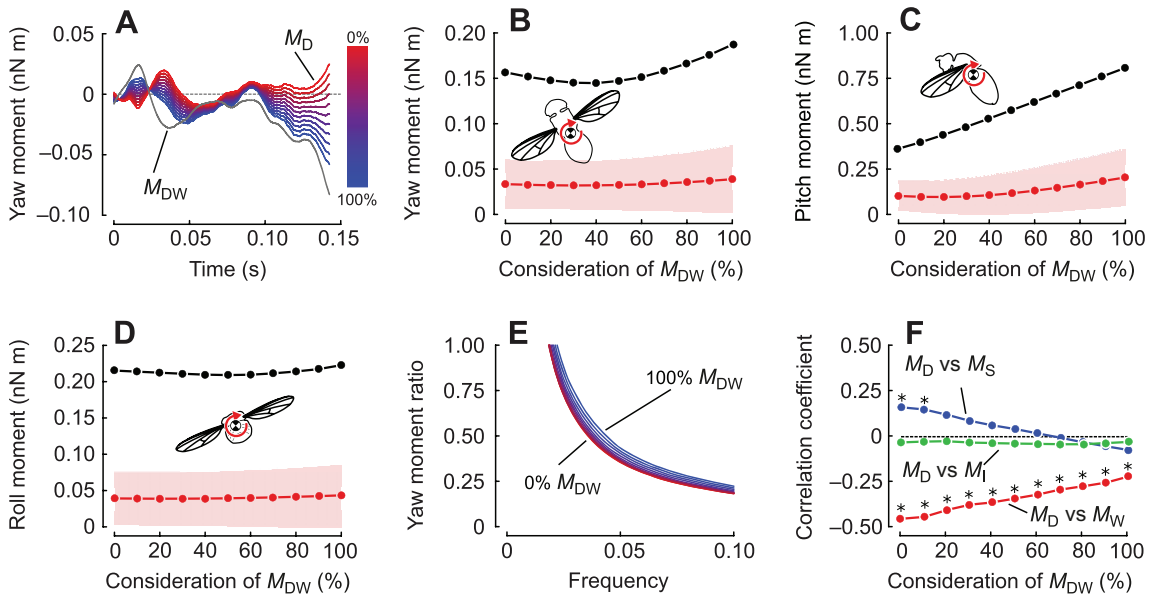

Fig. 7. Changes in moments caused by wing-flapping-induced flow (downwash). (A) Various time traces for drag-induced yaw moment (M_D) of the flight sequence in Fig. 2A with increasing consideration of downwash-induced moment M_{DW} (colour-coded; 0%, red; 100%, blue, 10% step width). (B–D) Moment means (red)±s.d. (red area) and the 1% largest moments of all flight sequences (black, N=24,596 samples of 81 flight sequences) plotted as a function of M_{DW}. Mean yaw is shown in B, mean pitch in C, and mean roll moment in D (N=81 sequences). (E) Ratio of drag- and wing-flapping-induced yaw moments. For colour coding see A. (F) Significance of downwash-induced yaw moments on correlation coefficients calculated in Figs 5 and 6. Coefficients are shown for drag- (M_D), mass-shift- (M_S), inertia- (M_I) and wing-flapping-induced moments (M_W). Asterisk indicates a significant difference from zero (one sample t-test, P<0.05). Mean standard deviations are ±0.4 (red), ±0.6 (blue) and ±0.4 (green, N=11).

Fig. 7F for coefficients of drag-induced yaw moments M_D versus M_S (blue) and M_D versus M_W (red). By contrast, the correlation coefficient of M_D versus M_I (yaw, green) is not affected by downwash and remains close to zero. We obtained similar results for roll moments (data not shown).

The significance of body posture on moments of inertia

Moment control in insects might also benefit from changes in moments of inertia around the three main body axes due to the active control of legs and abdomen (see Introduction section). To investigate the contribution of active motion, we numerically modelled the insect body as a solid cylinder with the mass of an average fruit fly and the hind legs as cylinders using typical lengths, diameters and masses of corresponding leg segments (cf. Materials and methods, Fig. 8A, Table 2). We first calculated the dependency of yaw, pitch and roll moments of inertia from body pitch angle in a model fly in which hind leg coxae and femurs are in a fixed position relative to the thorax, and without tibiae and tarsi (truncated flies, Fig. 8B). The data suggest that moments of inertia (yaw, roll) in fruit flies may vary 9-fold from ~0.11 to 0.99 ng m^2, depending on body pitch angle. By contrast, the moments of inertia due to mass motion of the hind leg tibia and tarsi are comparatively small compared with the moments derived from truncated flies, amounting to an increase in moments of ~5% in yaw (Fig. 8C), 0.8% in pitch (Fig. 8D) and 6% in roll (Fig. 8E).

For comparison, we also evaluated the maximum instantaneous increase of moments of inertia that a fly might reach during flight by mass motion of its legs, modelling truncated flies with tibia and tarsi but empirically derived hind leg extension angles that produced maximum moments of inertia. These data are plotted as red lines in Fig. 8C–E and confirm the small benefit of leg steering for the control of moments of inertia in fruit flies. On average, the theoretical prediction differs less than 1% increase in moments of inertia from data based on the kinematic reconstructions of leg angles of tibia and tarsi (black data points, Fig. 8C–E).

DISCUSSION

Steering by wings and body appendages

Our recorded flight sequences show a broad spectrum of flight behaviour in freely flying fruit flies, ranging from straight flight, sharp turns, backward and sideward flight to pronounced changes in flight altitude (Figs 1 and 2). The 3D reconstructed body posture, leg extension angles and abdomen bending highlight active components for body stability and directional control. This is evident from the elevated correlation coefficients between horizontal abdominal bending and leg extension angles (Pearson test, R=0.69), significant correlation coefficients between wing-flapping- and drag-induced yaw moments, and the correlation between wing-flapping- and inertia-induced yaw moments (Fig. 5A,D). Our findings are also consistent with previous experiments on abdomen control in tethered flying fruit flies (Zanker, 1987). The latter study also demonstrated that abdominal movements may not be caused by flow generated from wing flapping. Moreover, Table 1 and Figs 2 and 4 show that the various contributions of hind legs and abdomen to total moments are small and typically restricted to times at which wing-flapping-induced moments are small. Our moment ratio analyses suggest that steering by the hind legs and abdomen dominates moment control in only ~17% of total flight time (Fig. 4) and drag-induced moments are smallest compared with all other moment-generating mechanisms in fruit flies (Table 1). Thus, in analogy to ruddering of animals in water and air, the small contribution of drag due to proper motion of the legs rejects the idea that fruit flies may produce elevated moments by paddling movements of the hind legs (Ristroph et al., 2011).

Journal of Experimental Biology (2015) 218, 3295-3307 doi:10.1242/jeb.122408

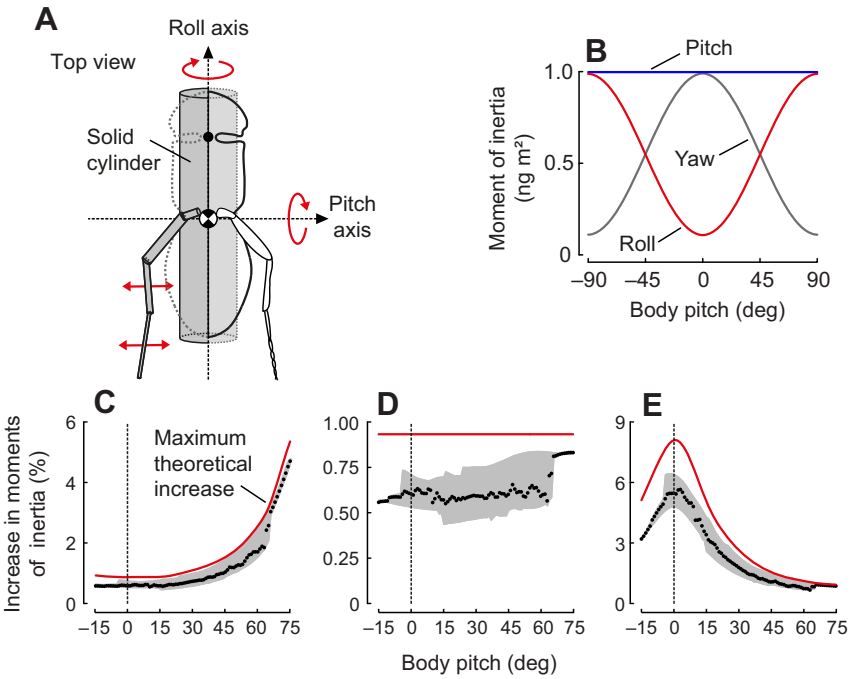

Fig. 8. Alteration in moments of inertia due to hind leg movements during flight. (A) Moment of inertia of yaw, pitch and roll was determined from a solid model cylinder with appropriate size and mass (cf. Materials and methods), rotating around the three body axes (cf. Fig. 1A). (B) Moments of inertia calculated for the model cylinder are plotted as a function of the cylinder's pitching angle, with zero the horizontal. (C–E) Relative increase in moments of inertia compared with B due to additional mass motion of tibia and tarsi of two hind legs. Binned moments of inertia within 1.0 deg pitch angle (black) are plotted for yaw in C, pitch in D and roll in E. *N*=24,596 data samples of 81 flight sequences. Grey area indicates the minimum–maximum range within a one-degree-bin and solid lines show a theoretical prediction of maximum increase based on selected hind leg extension angles. See text for more detailed information.

As outlined in the Materials and methods, estimation of wing-flapping-induced moments is crucial in our analysis on the relative contribution of abdomen- and leg-induced moments to total moments. Thus, we here compare our estimated wing-flapping-dominated total moments with the moments measured in tethered studies of *Drosophila* flying under various flight and visual feedback conditions. Table 1 shows that moments around the fly's yaw, pitch and roll axes peak at ∼11.2, 10.2 and 26.8 nN m. In tethered fruit flies flying under open-loop visual feedback conditions, for comparison, yaw varies between 3 and 8 nN m (Götz et al., 1979; Heisenberg and Wolf, 1979, 1988; Mayer et al., 1988) with peak values of 17 nN m (Tammero et al., 2004), pitch may reach 6 nN m (Blondeau and Heisenberg, 1982), and roll varies between 3 and 20 nN m (Blondeau and Heisenberg, 1982; Sugiura and Dickinson, 2009). Computational fluid dynamic modelling using free flight kinematics of fruit flies performing a saccadic turn reported a peak yaw moment of 2.0 nN m (mean ∼1.1 nN m, Ramamurti and Sandberg, 2007) and peak yaw moment derived from a robotic wing mimicking a saccadic turn amounted to ∼1.9 nN m in the same species (Fry et al., 2003). These values are broadly similar to the values shown in Table 1, which gives credence to the method used in the present study for estimation of total moment.

Coherence of steering

Previous studies on flight control in tethered flies suggest that hind leg steering during optomotor yaw response reinforces wing-flapping-induced moments by strongly increasing (decreasing) the leg extension angle on the inner (outer) side of an intended yaw turn (Zanker, 1988a, 1991). The author proposed that this synergy increases the fly's agility and manoeuvrability, which may, in turn, increase survival rate during aerial predation by dragonflies (Combes et al., 2012). Our data reject the above hypothesis for unrestrained flying fruit flies. We found no preference for the idea that leg extension and abdomen bending angles coherently support turning direction of the animal. In contrast to leg kinematics, we even found that sequence-averaged yaw moments due to drag on legs and abdomen significantly inhibit rather than support wing-flapping-induced moments (negative correlation coefficient in Fig. 5D), which might enhance posture stability. The same holds for mass-shift-induced moments, suggesting a synergistic function of motor pathways to hind legs and abdomen (Fig. 5E). However, counter moments during yaw turning might also result from an increase in local velocities at the hind leg on the outer side of a flight curve, despite its smaller leg extension angle. Data indeed show that an increase in rotational velocity of the body is positively correlated with an increase in hind leg velocity on the outer side of a turn (Pearson correlation, R=0.77). Therefore, while the above mechanism might passively restrict angular velocity in turning flight caused by aerodynamic damping, flies actively shift their centre of mass (abdomen bending) to the body side that counteracts moments generated by wing flapping. The latter mechanism is independent of angular turning rate because it solely relies on

Table 2. Morphological measures of *Drosophila* hind leg segments

	Coxa	Femur–trochanter	Tibia	Tarsus
Length (μm)	249±30.4	635±24.3	659±23.3	742±25.6
Mean width (μm)	120±9.16	119±5.18	68.3±2.78	39.8±1.88
Area (×10^3 μm^2)	29.9±5.12	75.4±4.76	45.0±2.91	29.5±1.83
Volume (×10^6 μm^3)	3.02±0.75	7.21±0.74	2.51±0.25	1.01±0.11
Centre of mass (%)	38.5±2.24	44.5±1.32	58.6±1.02	34.8±2.63
Centre of area (%)	43.9±1.29	47.0±0.79	54.8±0.64	42.1±1.42

Mass of each leg segment was estimated from its relative volume, determined from 21 blade elements and using total leg mass. The position of centre of mass is given as a fraction of segment length with 0% the proximal segment end. Mean±s.d., *N*=11 hind legs from 11 flies.

Journal of Experimental Biology (2015) 218, 3295-3307 doi:10.1242/jeb.122408

changes in the length of the moment arm between the fly's centre of mass and the centre of flight force at mid up- or downstroke (Fig. 2C).

The apparent synergy between drag- and mass-shift-induced moments and their attenuation on wing-flapping-induced moments is also supported by its positive correlation coefficients during yaw and roll control (Fig. 6A,D, yaw). This result is consistent with previous findings on the coherence of leg and abdominal movements in the tethered housefly (Zanker, 1991). The latter study demonstrated that hind legs and abdomen move in-phase and in the same direction during vision-controlled flight. However, our finding that positive (yaw, 51%; roll, 47%) and negative moment coherence (yaw, 49%; roll, 53% flight time) occur with approximately the same frequency suggests a highly flexible system with quite independently acting system components for moment control.

Significance of induced flow

This study considered induced flow (wing downwash) in detail because of its unsettled contribution to drag-induced moments. Wings and legs are mechanically connected and thus any increase in downwash-induced force pushing legs and body downward in the vertical attenuates body lift production by wing flapping via the mechanical link. After its initial acceleration, downwash velocity and vorticity are thought to decrease with increasing distance from the wings' stroke plane owing to the viscous forces of the surrounding air. However, owing to the small distance of less than a millimetre between stroke plane and legs, this effect is assumed to be small. The different lengths of moment arm for wing-flapping- and drag-induced moments do not allow simple predictions of moment control by changes in downwash velocity. We tackled this problem by calculation of moments, in which we considered downwash as an intervortex stream with uniform velocity but various strengths. Our results in Fig. 7 suggest that induced flow alters total moments depending on the rotational axis: roll moment is rather independent of induced flow and changes only up to 5%, while yaw moments may potentially change up to 22% and pitch moments up to 56% of total moment. Despite the pronounced percentage changes, consideration of moments caused by induced flow does not alter the main result of this study; however, these changes might matter when wing-induced moments are relatively small. Collectively, the exact contribution of downwash to body posture and turning control remains somewhat unclear and requires further investigation.

Significance of body posture on moments of inertia

An alternative benefit of active control of legs and abdomen during manoeuvring flight resides in the associated changes in moments of inertia around the three body axes. Since moments of inertia depend on mass distribution, any changes in vertical and horizontal position of legs and abdomen may potentially modulate this measure. It has previously been shown that orchid bees flying in turbulent air laterally extend their hind legs. This increases drag by ∼30% but also moments of inertia around the animal's roll axis by up to 53%, which, in turn, should enhance flight stability (Combes and Dudley, 2009). Owing to the smaller hind leg mass in fruit flies of ∼9.42 µg or 1.2±0.3% body mass compared with orchid bees (5.9% body mass), the changes in moments of inertia are comparatively small: hind leg motion in *Drosophila* alters moments of inertia of not more than 6% (Fig. 8). Moreover, compared with a model fruit fly without hind leg tibia and tarsi, moments of inertia during yaw, pitch and roll steering may not increase more than 8% of the moments of inertia of the body trunk. The largest benefit of hind leg control in fruit flies is on roll stability, which is consistent with data obtained from the orchid bee. Consequently, leg extension in small insects such as the fruit fly appears to be of little significance for posture stability but, nevertheless, might slightly enhance stability of animals flying under turbulent environmental conditions that require elevated steering performance.

Conclusions

This study shows how freely flying fruit flies control their flight path by synergistic action of three independently working motor control systems, enhancing the degrees of freedom for heading and posture control. In general, turning moments produced by wing motion dominate both: moments produced by aerodynamic drag on body and hind legs and positional changes of the fly's centre of mass by movements of hind legs and abdomen. Their small contribution suggests that fruit flies use their hind legs and abdomen to fine-tune moments for flight rather than to produce large moments required during flight saccades or optomotor responses. The latter highlights the potential importance of leg and abdominal steering for aerial manoeuvring during straight flight. Nevertheless, while maximum body-drag-induced yaw moments (0.19 nN m) correspond to a unilateral wing stroke equivalent of only ∼0.7 deg amplitude, maximum alteration in positional change of centre of body mass (2.6 nN m) converts into a pronounced unilateral change in stroke amplitude of 8.8 deg (Hesselberg and Lehmann, 2007). Alternatively, motion control of body appendages might be part of the insect's trimming reflexes to trim out bilateral imbalances in forces and moments during flight. These imbalances may result from unilateral aerodynamic effective changes such as wing damage, abnormal asymmetries of the flight apparatus, and an imbalance in muscle mechanical power output and control for wing motion (Bender and Dickinson, 2006; Hesselberg and Lehmann, 2009). In this regard, legs in insects are aerodynamic rudders, similar to those that correct for the counter torque from the propeller in airplanes.

Seen in a larger context, drag-based leg control in flying *Drosophila* appears similar to the function of middle and hind legs in apterygote hexapods, such as wingless gliding ants, for aerial manoeuvrability and gliding performance (Yanoviak et al., 2009, 2010). From an evolutionary point of view, fruit flies might thus have inherited leg and abdominal motor control systems from their wingless ancestors. The small benefit of leg control in *Drosophila* on moments of inertia, however, runs counter to the idea that leg steering has primarily evolved as a mechanism to enhance posture stability. In this respect, the male orchid bee might be an exception because its hind leg tibia is greatly enlarged compared with that of other insect species in order to collect scents (Combes and Dudley, 2009).

MATERIALS AND METHODS

High-speed video recording inside a free-flight arena

The flies were scored in a free-flight arena, allowing automated recordings of body posture, abdominal bending and hind leg motion using three-dimensional high-speed video (Shishkin et al., 2012, Fig. 9). To stimulate 0.1 µg fluorescence dye markers on the fly (Fig. 9B,C), we flashed UV-emitting diodes with 60 µs short voltage pulses. Position accuracy of the video-tracked markers was within ±30 µm and images were recorded inside a volume of 20 mm width×20 mm length×25 mm height at 3500 Hz frame rate (Hedrick, 2008). We scored 81 flight sequences of 14 female, 3- to 5-day-old wild-type *Drosophila melanogaster* (Canton S) with an average body mass of 1.26±0.04 mg. Total flight time of all analysed sequences was 7.03 s, with individual sequences ranging from 15.7 ms to 355 ms, and mean ambient temperature was 23.6°C.

Journal of Experimental Biology (2015) 218, 3295-3307 doi:10.1242/jeb.122408

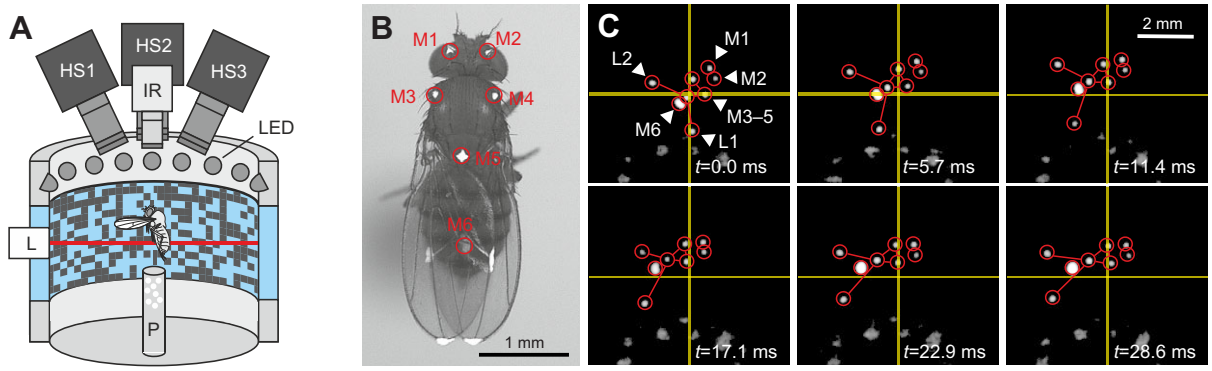

Fig. 9. Video reconstruction of body markers in freely flying fruit flies. (A) Free-flight arena (not to scale). HS, high-speed camera; IR, infrared light camera; L, infrared laser sheet; LED, ultraviolet light-emitting diodes; P, starting platform. (B) Fly with fluorescent markers (M1–M6). Note that the image shows an animal with marked wings instead of marked hind legs. (C) Time series of video images recorded by high-speed camera HS2. Images show fluorescent markers with tagged positions of the body (M1–5), abdomen (M6) and hind leg tarsi (L1,L2). The white blobs in the lower part of the images result from fluorescent markers on the starting platform. The time interval of 5.7 ms corresponds to 20 recorded frames of the video sequence.

Positional reconstruction of leg segments

We simplified the reconstruction of leg extension angles, performing pre-tests on leg movements in tethered flying flies (N=7, Fig. 10). A conventional infra-red video camera recorded the animal from lateral (V, vertical angle) and the bottom (H, horizontal angle), while the fly changed wing and leg motion in response to a visual stimulus. We scored the angles between (1) femur and tibia (δ), (2) tibia and tarsi (ε), (3) femur and a connection line through the femur-tibia joint and the fifth tarsal segment (ζ) and (4) femur and longitudinal body axis (κ). From these angles, we calculated mean angles and variances (N=10 images of each fly and camera view) that yielded: 74.2±36.7 deg (δ_V), 125±18.3 deg (δ_H), 128±25.9 deg (ε_V), 161±10.5 deg (ε_H), 105±27.5 deg (ζ_V), 143±11.9 deg (ζ_H), 58.4±2.4 deg (κ_V) and 45.9±4.8 deg (κ_H).

These measurements and subsequent correlation analyses suggested: (1) the small standard deviations of angle κ indicate that coxa and femur move only little during steering, thus κ was considered to be a constant and the tibia–femur joint position determined from thoracic fluorescent markers; (2) the high standard deviation of δ indicates that the animal predominately alters this angle during leg steering; (3) angle δ significantly depends on angle ζ (Pearson test, vertical, P<0.001, R=0.98, N=70; horizontal, P<0.001, R=0.66, N=422); (4) angle ε_V linearly depends on δ_V (Pearson test, P<0.001, R=0.82, N=70); and (5) angle ε_H is not linearly correlated with δ_H and thus considered to be a constant (Pearson test, P=0.22, R=0.06, N=422). From the leg extension angles ζ in free flight and linear regression analyses on leg angles in tethered animals, we determined remaining angles and leg positions using the equations:

$$\delta_V\,(\text{deg}) = 1.39\,\zeta_V\,(\text{deg}) - 68.62\,(\text{deg}), \quad (1)$$

$$\delta_H\,(\text{deg}) = 0.87\,\zeta_H\,(\text{deg}) + 10.75\,(\text{deg}), \quad (2)$$

$$\varepsilon_V\,(\text{deg}) = 0.77\,\zeta_V\,(\text{deg}) + 46.90\,(\text{deg}). \quad (3)$$

Estimation of aerodynamic drag on legs and body trunk

Body appendages and thus the modelled cylinders experience drag by cross flow and lift by flow parallel to the longitudinal cylinder axis. In the latter case, however, the complex zigzag geometry of the leg segments with positive and negative inclination results in a small overall angle of attack (Fig. 2B). In addition, peak lift coefficient of cylinders is only 11–20% of the maximum drag coefficient at Reynolds numbers (Re) between 7 and 20 (Babu and Mahesh, 2008; Vakil and Green, 2009). Together, this results in at least 35 times less instantaneous lift than drag for the example in Fig. 2. Thus, we did not further consider lift-induced moments. We determined aerodynamic drag using a combined approach, in which we estimated the aerodynamic effective, local frontal area with respect to the oncoming flow, the local air flow vector from kinematic reconstruction, an experimentally validated, velocity-dependent and thus Re-dependent drag coefficient, and Eqn 7. Drag was estimated separately for each leg and body segment,

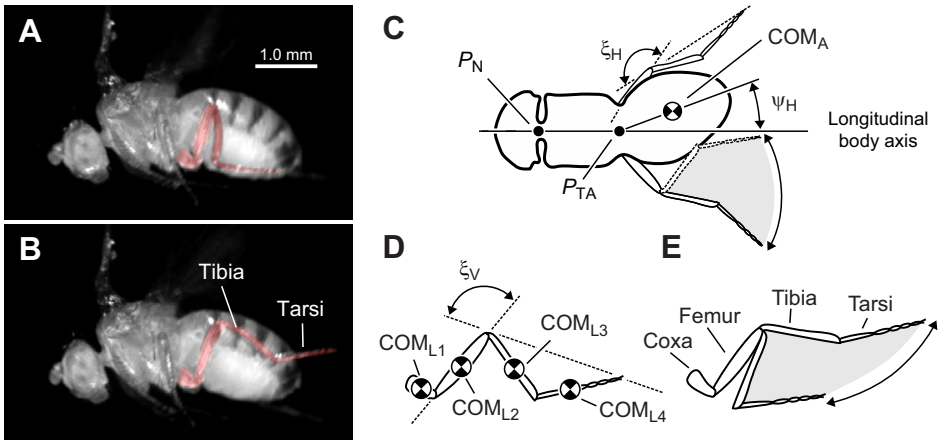

Fig. 10. Abdomen bending and hind leg extension angle during manoeuvring flight. (A,B) Side view of a tethered fruit fly responding to the motion of a visual stimulus. Fruit flies mainly steer by changes in wing motion, abdominal movement, and by moving tibia and tarsi of the hind legs (red). (C,D) Horizontal and vertical leg extension angles ζ_H and ζ_V were reconstructed from the 3D position of the distal tarsal segment and the angular position of the femur, respectively. Abdominal deflection angles ψ_H and ψ_V were derived from the animal longitudinal axis, the abdomen's centre of mass COM_A and the abdominal point of rotation P_{TA} (cf. Fig. 1A). Mass of abdomen and hind legs COM_{L1}–COM_{L4} including the combined mass of head and thorax were estimated from weight measurements and using an elementary blade approach. P_N, position of the neck connective in the sagittal plane.

Journal of Experimental Biology

Journal of Experimental Biology (2015) 218, 3295-3307 doi:10.1242/jeb.122408

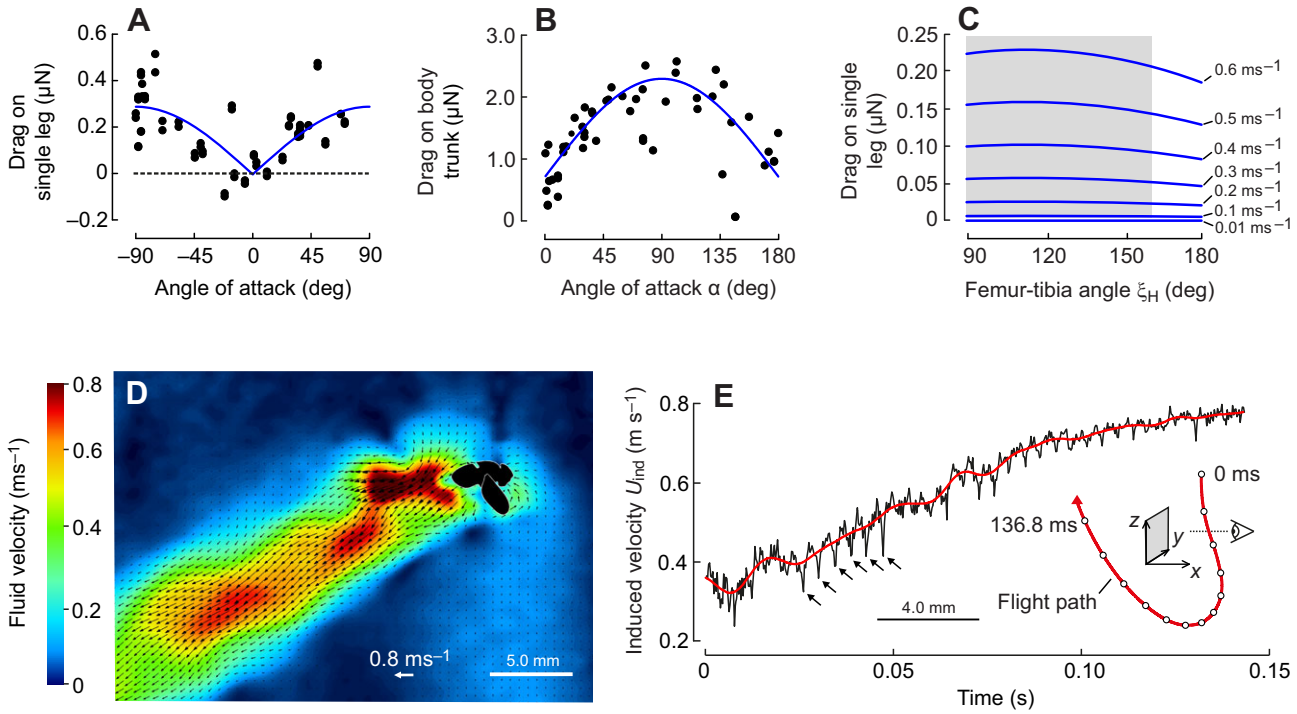

Fig. 11. Experimental evaluation of drag coefficients and wake velocity distribution in *Drosophila*. (A,B) The coefficients were estimated from drag measurements of isolated legs and truncated corpses of fruit flies (without legs and wings) mounted in a low Reynolds number, laminar wind tunnel. Drag (D, black) of a single, stretched out hind leg in A and body trunk in B plotted as the function of angle of attack α with respect to the oncoming flow. Blue, sinusoidal fit to data; left, D=–0.0043+0.292 |sinα|; right, D=0.709+1.585 sinα. (C) Calculated drag of a single leg during free flight with mean ζ_V=105 deg (N=81 flight sequences, Fig. 10), and depending on ζ_H and the horizontal component of u_{leg}. See Fig. 2 for leg configuration and Material and methods for angles. Grey area indicates the leg's active steering range (see Fig. 1E,F). Maximum relative change in drag within the grey area is 9.5% for each u_{leg}. (D) Wake velocities measured in the parasagittal plane of a tethered flying fly. The snapshot shows wake and fly from lateral and was recorded by digital particle image velocimetry as described in a previous study (Lehmann, 2012). Note that velocity vectors close to the insect body are reconstructed from surrounding vectors because of laser light reflections at the fly's cuticle. Tethering (pitch) angle was approximately zero and induced flow is thus directed sideways. For comparison, vertical, lift-supporting, mean induced velocity based on Eqn 5 was 0.64±0.13 m s^{-1} and the 1% maximum in each sequence 0.69±0.12 m s^{-1} (N=81 flight sequences). (E) Induced velocity for the flight sequence shown in Fig. 2. Raw data (black) indicate stroke cycle synchronous alteration in velocity (arrows). Smoothed data are plotted in red.

modelling each segment as a solid, rigid cylinder with appropriate mean length, width and total mass. For cylinders, White (1974) suggested a *Re*-based, empirical approximation of drag coefficient, C_D, written as:

$$C_D = 1 + 10 \cdot Re^{-2/3}, \quad (4)$$

in which *Re* is derived from the local velocity of the segment and a characteristic length of twice the cylinder radius. Compared with previous measurements of drag coefficients on cylinders at cross wind, Eqn 4 yields negligible differences at *Re* between 1 and 10 (Tritton, 1959). Mean *Re* of a single leg is ~1.9 (235 mm s^{-1} body velocity, cylinder radius 60 μm, 15×10^{-6} m^2 s^{-1} kinematic viscosity). Besides body motion, local velocity also depends on induced velocity (u_{ind}, downwash) generated by wing flapping, which was calculated by Ellington (1984e) and Usherwood and Lehmann (2008):

$$u_{ind} = \sqrt{\frac{L}{2\rho A}}, \quad (5)$$

where L is body lift, ρ is the density of air and A is the area covered by the beating wings (Fig. 11D). We approximated the latter measure using a mean wing beat amplitude of 162 deg and wing length of 2.5 mm (Lehmann and Dickinson, 1998). Instantaneous body lift was calculated from translational movements of the fly and a previously derived vertical damping coefficient C_{vert} of 54.8 mg s^{-1}, written as:

$$L(t) = m_b \cdot \dot{u}_{vert}(t) + C_{vert} \cdot u_{vert}(t) + m_b \boldsymbol{g}, \quad (6)$$

where m_b is the body mass, $\boldsymbol{g}$ is the gravitational constant and t is time.

To experimentally validate *Re*-dependent drag, we determined drag on body appendages in a 1.05 m s^{-1} laminar flow wind tunnel and using a laser balance (Lehmann and Dickinson, 1998). *Re* varied between ~2.8 (tarsi) and 8.3 (femur, Table 2). We removed hind legs from female flies, mounted them on a flat surface and dried them overnight in a stretched position to avoid changes in leg posture due to joint flexing. We mounted 7 legs at equal distance of 1.0 mm, orthogonal to a tungsten wire (127 μm diameter), positioned the wire with the legs normal to the air flow, and rotated it to measure the legs' drag at various angles of attack (Fig. 11). Similarly, we estimated yaw angle-dependent body drag on a fly trunk, removing wings and legs from a dead animal and gluing the trunk with the longitudinal body axis oriented normally to the wire. Drag components due to the tungsten wire were subtracted from the measures. We subsequently fitted a sinusoidal curve to the data and estimated the drag coefficient C_D using fitted values and the equation:

$$C_D = \frac{2D}{\rho u_{leg}^2 S}, \quad (7)$$

in which D is drag, u_{leg} is the velocity at the centre of area of the body segment and S is the frontal surface area of the segment facing the flow. At 90 deg angle of attack at which the flow is normal to hind legs and body trunk, drag coefficients were 2.96 and 1.41, respectively. For comparison, drag coefficients for hind leg and body trunk, modelled as a simple cylinder in Eqn 4 at comparable *Re*, are 3.14 and 1.44, respectively, which is only 2–6% higher than the measured coefficients (Fig. 11).

Estimation of moments

Moments around the fly's yaw, pitch and roll axes rely on at least four, independently acting mechanisms: moments due to (1) lift (perpendicular) and drag (parallel to relative flow) acting on the flapping wings; (2) drag on hind legs, thorax, head and abdomen; (3) changes in moment arm of wing flapping-induced moments by positional alterations of the fly's centre of mass; and (4) active mass movements of hind legs and abdomen. In contrast to drag- and mass-shift-induced moments, we derived wing-induced moments from (1) instantaneous measures of body motion; (2) moments of inertia I, with the body and hind leg segments approximated as cylinders (see Eqns 10–15); and (3) previously derived damping coefficients of the wings for body rotation in freely flying fruit flies C_{rot}. These coefficients are 176 ng m^2 s^{-1} for yaw, 204 ng m^2 s^{-1} for pitch and 352 ng m^2 s^{-1} for roll (N=170 flies, Shishkin et al., 2012). Total instantaneous moment, M_{M}, around the centre of body mass thus equals:

$$M_{\mathrm{M}}(t) = I\dot{\omega}(t) + C_{\mathrm{rot}}\omega(t), \quad (8)$$

with ω the rotational, angular velocity of the animal (Hesselberg and Lehmann, 2007). Wing-induced moments M_{W} for posture and heading control were then calculated by subtraction of the remaining components, which may be written as:

$$M_{\mathrm{W}}(t) = M_{\mathrm{M}}(t) - M_{\mathrm{D}}(t) - M_{\mathrm{S}}(t) - M_{\mathrm{I}}(t) - M_{\mathrm{DW}}(t), \quad (9)$$

where M_{D} is body-drag-induced, M_{S} is body-mass-shift-induced, M_{I} is inertia-induced and M_{DW} is downwash-induced moment. Downwash-induced moments were only considered in the analysis shown in Fig. 7.

We calculated drag-induced moments M_{D} from the x-, y- and z-components of the cross product between drag on body, abdomen and hind legs using Eqn 7 and the corresponding moment arm. The local flow vector was derived from the vector sum of body motion, active leg motion, and, in cases in which we considered downwash, from induced velocity and instantaneous body lift in Eqns 5 and 6, respectively. To derive abdomen-induced mass shift moments M_{S}, we used a simplified approach: we defined the moment arm as the distance between the aerodynamic centre of force of each wing at 56% wing length and the fly's centre of body mass (Ramamurti and Sandberg, 2007). Since this distance varies throughout the wing flapping cycle, we used a mean moment arm at mid half stroke, when the wing's longitudinal axis was in the horizontal and normal to the fly's longitudinal body axis (Fig. 2C). At mid half stroke and zero vertical body velocity, instantaneous vertical lift of each wing equals to ∼6.18 µN (m_{b}=1.26 mg, cf. Eqn 6), and instantaneous horizontal drag of each wing is ∼2.25 µN. We calculated the latter value according to: (1) the drag characteristics of a robotic fruit fly wing (Re=134, Dickinson et al., 1999); (2) mean wing velocity at the wing's centre of force; (3) mean wing area of one wing of 1.74 mm^2 of *Drosophila*; and (4) using Eqn 7.

Estimation of moments of inertia

We estimated the fly's moments of inertia by modelling the body trunk including fore legs, middle legs and the hind leg coxae and femurs as a single object, composed of solid cylinders (Fig. 8A). By contrast, hind leg tibia and tarsi were modelled separately as moving cylinders with appropriate mass. Total mass of a hind leg was 9.42±2.85 µg (N=4 groups of 10 legs each) and mean mass for hind leg coxa, femur, tibia and tarsi was 2.02, 5.02, 1.72 and 0.66 µg, respectively (Table 2). The yaw, pitch and roll moments of inertia of the cylinder were derived from the following equation:

$$I = I_a\cos^2(\phi_a) + I_b\cos^2(\phi_b) + I_c\cos^2(\phi_c) + m_{\mathrm{cyl}}\,d^2, \quad (10)$$

where I_a, I_b and I_c are the cylinder's principal moments of inertia, ϕ_a, ϕ_b and ϕ_c are the angles between the axis of rotation and the cylinder's principal axes a, b and c, respectively, m_{cyl} is the cylinder mass and d is the distance between the centre of mass and the axis of rotation (parallel axis theorem). We may write the principal moments of inertia for the principal axis a thus as:

$$I_a = \frac{m_{\mathrm{cyl}} \cdot r^2}{2}, \quad (11)$$

and for the axes b and c as:

$$I_b = I_c = \frac{m_{\mathrm{cyl}} \cdot r^2}{4} + \frac{m_{\mathrm{cyl}} \cdot l^2}{12}, \quad (12)$$

where r is the cylinder radius and l is the cylinder length. The yaw and roll axes of the body trunk cylinder are within the a–c plane and the pitch axis is the cylinder b-axis. This leads to the following set of equations for moments of inertia of the body trunk about the three axes, i.e. for yaw:

$$I_{\mathrm{yaw}} = (1 + \sin^2\langle\chi\rangle)\frac{m_{\mathrm{cyl}} \cdot r^2}{4} + \cos^2\langle\chi\rangle\frac{m_{\mathrm{cyl}} \cdot l^2}{12}, \quad (13)$$

for pitch:

$$I_{\mathrm{pitch}} = \frac{m_{\mathrm{cyl}} \cdot r^2}{4} + \frac{m_{\mathrm{cyl}} \cdot l^2}{12}, \quad (14)$$

and for roll:

$$I_{\mathrm{roll}} = (1 + \cos^2\langle\chi\rangle)\frac{m_{\mathrm{cyl}} \cdot r^2}{4} + \sin^2\langle\chi\rangle\frac{m_{\mathrm{cyl}} \cdot l^2}{12}, \quad (15)$$

with χ the pitch angle. Eventually, to achieve total moments of inertia, we calculated the moments of inertia for hind leg tibia and tarsi using Eqn 10 and added these values to the moments of inertia of the body trunk.

Statistics

If not mentioned otherwise, all data are given as means±s.d. throughout the manuscript.

Acknowledgements

We thank Peter Schützner for providing flight data and Ursula Seifert for her comments on the manuscript.

Competing interests

The authors declare no competing or financial interests.

Author contributions

R.B. and F.O.L. designed the research; R.B. performed the research and analysed data; R.B. and F.O.L. wrote the manuscript.

Funding

This research was supported by a grant from the German Science Foundation [LE905/9-3 to F.O.L.].

References

Alexander, R. M. (2003). *Principles of Animal Locomotion*. Princeton, NJ: Princeton University Press.

Arbas, E. A. (1986). Control of hindlimb posture by wind-sensitive hairs and antennae during locust flight. *J. Comp. Physiol. A* **159**, 849-857.

Babu, P. and Mahesh, K. (2008). Aerodynamic loads on cactus-shaped cylinders at low Reynolds numbers. *Phys. Fluids* **20**, 035112.

Bender, J. A. and Dickinson, M. H. (2006). A comparison of visual and haltere-mediated feedback in the control of body saccades in *Drosophila melanogaster*. *J. Exp. Biol.* **209**, 4597-4606.

Blondeau, J. and Heisenberg, M. (1982). The three-dimensional optomotor torque system of *Drosophila melanogaster*. *J. Comp. Physiol. A* **145**, 321-329.

Burrows, M., Cullen, D. A., Dorosenko, M. and Sutton, G. P. (2015). Mantises exchange angular momentum between three rotating body parts to jump precisely to targets. *Curr. Biol.* **25**, 786-789.

Camhi, J. M. (1970a). Sensory control of abdomen posture in flying locusts. *J. Exp. Biol.* **52**, 533-537.

Camhi, J. M. (1970b). Yaw-correcting postural changes in locusts. *J. Exp. Biol.* **52**, 519-531.

Cheng, B., Deng, X. and Hedrick, T. L. (2011). The mechanics and control of pitching manoeuvres in a freely flying hawkmoth (*Manduca sexta*). *J. Exp. Biol.* **214**, 4092-4106.

Combes, S. A. and Dudley, R. (2009). Turbulence-driven instabilities limit insect flight performance. *Proc. Nat. Acad. Sci.* **106**, 9105-9108.

Combes, S. A., Rundle, D. E., Iwasaki, J. M. and Crall, J. D. (2012a). Linking biomechanics and ecology through predator-prey interactions: flight performance of dragonflies and their prey. *J. Exp. Biol.* **215**, 903-913.

Cook, M. V. and Spottiswoode, M. (2006). Modelling the flight dynamics of the hang glider. *Aero. J.* **110**, 1-20.

Journal of Experimental Biology

Dickinson, M. H., Lehmann, F.-O. and Sane, S. (1999). Wing rotation and the aerodynamic basis of insect flight. *Science* **284**, 1954-1960.
Dyhr, J. P., Morgansen, K. A., Daniel, T. L. and Cowan, N. J. (2013). Flexible strategies for flight control: an active role for the abdomen. *J. Exp. Biol.* **216**, 1523-1536.
Ellington, C. P. (1984a). The aerodynamics of hovering insect flight. IV. Aerodynamic mechanisms. *Philos. Trans. R. Soc. B Biol. Sci.* **305**, 79-113.
Ellington, C. P. (1984b). The aerodynamics of hovering insect flight. VI. Lift and power requirements. *Philos. Trans. R. Soc. B Biol. Sci.* **305**, 145-181.
Ellington, C. P. (1984c). The aerodynamics of hovering insect flight. III. Kinematics. *Proc. R. Soc. B Biol. Sci.* **305**, 41-78.
Ellington, C. P. (1984d). The aerodynamics of hovering insect flight. II. Morphological parameters. *Philos. Trans. R. Soc. B Biol. Sci.* **305**, 17-40.
Ellington, C. P. (1984e). The aerodynamics of hovering insect flight. V. A vortex theory. *Philos. Trans. R. Soc. B Biol. Sci.* **305**, 115-144.
Ellington, C. P. (1991). Limitations on animal flight performance. *J. Exp. Biol.* **160**, 71-91.
Fry, S. N., Sayaman, R. and Dickinson, M. H. (2003). The aerodynamics of free-flight maneuvers in *Drosophila*. *Science* **300**, 495-498.
Frye, M. A. (2001). Effects of stretch receptor ablation on the optomotor control of lift in the hawkmoth *Manduca sexta*. *J. Exp. Biol.* **204**, 3683-3691.
Götz, K. G., Hengstenberg, B. and Biesinger, R. (1979). Optomotor control of wing beat and body posture in *Drosophila*. *Biol. Cybern*. **35**, 101-112.
Hedrick, T. L. (2008). Software techniques for two- and three-dimensional kinematic measurements of biological and biomimetic systems. *Bioinspir. Biomim.* **3**, 034001.
Hedrick, T. L. and Daniel, T. L. (2006). Flight control in the hawkmoth Manduca sexta: the inverse problem of hovering. *J. Exp. Biol.* **209**, 3114-3130.
Heisenberg, M. and Wolf, R. (1979). On the fine structure of yaw torque in visual flight orientation of *Drosophila melanogaster*. *J. Comp. Physiol. A* **130**, 113-130.
Heisenberg, M. and Wolf, R. (1988). Reafferent control of optomotor yaw torque in *Drosophila melanogaster*. *J. Comp. Physiol. A* **163**, 373-388.
Hesselberg, T. and Lehmann, F.-O. (2007). Turning behaviour depends on frictional damping in the fruit fly *Drosophila*. *J. Exp. Biol.* **210**, 4319-4334.
Hesselberg, T. and Lehmann, F.-O. (2009). The role of experience in flight behaviour of *Drosophila*. *J. Exp. Biol.* **212**, 3377-3386.
Hinterwirth, A. J. and Daniel, T. L. (2010). Antennae in the hawkmoth *Manduca sexta* (Lepidoptera, Sphingidae) mediate abdominal flexion in response to mechanical stimuli. *J. Comp. Physiol. A* **196**, 947-956.
Jusufi, A., Goldman, D. I., Revzen, S. and Full, R. J. (2008). Active tails enhance arboreal acrobatics in geckos. *Proc. Nat. Acad. Sci.* **105**, 4215-4219.
Kane, T. R. and Scher, M. P. (1970). Human self-rotation by means of limb movements. *J. Biomech.* **3**, 39-49.
Kulwicki, P. V., Schlei, E. J. and Vergamini, P. L. (1962). Weightless Man: Self-Rotation Techniques. Ohio: Air Force Aerospace Medical Research Lab Wright-Patterson Air Force Base.
Laouris, Y., Kalli-Laouri, J. and Schwartze, P. (1990). The postnatal development of the air-righting reaction in albino rats. Quantitative analysis of normal development and the effect of preventing neck-torso and torso-pelvis rotations. *Behav. Brain Res.* **37**, 37-44.
Lehmann, F.-O. (2012). Wake structure and vortex development in flight of fruit flies using high-speed particle image velocimetry. In *Nature-Inspired Fluid Mechanics* (ed. C. Tropea and H. Bleckmann), pp. 65-80. Berlin; Heidelberg: Springer.
Lehmann, F.-O. and Dickinson, M. H. (1998). The control of wing kinematics and flight forces in fruit flies (*Drosophila* spp.). *J. Exp. Biol.* **201**, 385-401.
Libby, T., Moore, T. Y., Chang-Siu, E., Li, D., Cohen, D. J., Jusufi, A. and Full, R. J. (2012). Tail-assisted pitch control in lizards, robots and dinosaurs. *Nature* **481**, 181-184.
Mayer, M., Vogtmann, K., Bausenwein, B., Wolf, R. and Heisenberg, M. (1988). Flight control during 'free yaw turns' in *Drosophila melanogaster*. *J. Comp. Physiol. A* **163**, 389-399.
Pennycuick, C. J. (1960). Gliding flight of the fulmar petrel. *J. Exp. Biol.* **37**, 330-338.
Pennycuick, C. J. (1968). A wind-tunnel study of gliding flight in the pigeon *Columba livia*. *J. Exp. Biol.* **49**, 509-526.
Pennycuick, C. J. (1971). Control of gliding angle in Rüppell's griffon vulture *Gyps rüppellii*. *J. Exp. Biol.* **55**, 39-46.
Ramamurti, R. and Sandberg, W. C. (2007). A computational investigation of the three-dimensional unsteady aerodynamics of *Drosophila* hovering and maneuvering. *J. Exp. Biol.* **210**, 881-896.
Ristroph, L., Bergou, A. J., Guckenheimer, J., Wang, Z. J. and Cohen, I. (2011). Paddling mode of forward flight in insects. *Phys. Rev. Lett.* **106**, 178103.
Shishkin, A., Schützner, P., Wagner, C. and Lehmann, F.-O. (2012). Experimental quantification and numerical simulation of unsteady flow conditions during free flight maneuvers in insects. In *Nature-Inspired Fluid Mechanics* (ed. C. Tropea and H. Bleckmann), pp. 81-99. Berlin; Heidelberg: Springer.
Sugiura, H. and Dickinson, M. H. (2009). The generation of forces and moments during visual-evoked steering maneuvers in flying *Drosophila*. *PLoS* ONE **4**, e4883.
Tammero, L. F., Frye, M. A. and Dickinson, M. H. (2004). Spatial organization of visuomotor reflexes in *Drosophila*. *J. Exp. Biol.* **207**, 113-122.
Tritton, D. J. (1959). Experiments on the flow past a circular cylinder at low Reynolds numbers. *J. Fluid Mech.* **6**, 547-567.
Usherwood, J. R. and Lehmann, F.-O. (2008). Phasing of dragonfly wings can improve aerodynamic efficiency by removing swirl. *J. R. Soc. Interface* **5**, 1303-1307.
Vakil, A. and Green, S. I. (2009). Drag and lift coefficients of inclined finite circular cylinders at moderate Reynolds numbers. *Comput. Fluids* **38**, 1771-1781.
White, F. M. (1974). Viscous Fluid Flow. New York, US: McGraw-Hill.
Yanoviak, S. P., Kaspari, M. and Dudley, R. (2009). Gliding hexapods and the origins of insect aerial behaviour. *Biol. Lett.* **5**, 510-512.
Yanoviak, S. P., Munk, Y., Kaspari, M. and Dudley, R. (2010). Aerial manoeuvrability in wingless gliding ants (*Cephalotes atratus*). *Proc. R. Soc. Lond. B* **277**, 2199-2204.
Zanker, J. M. (1987). *Über die Flugkrafterzeugung und Flugkraftsteuerung der Fruchtfliege Drosophila melanogaster*, p. 118. Tübingen: Eberhard-Karls-Universität Tübingen.
Zanker, J. M. (1988a). How does lateral abdomen deflection contribute to flight control of *Drosophila melanogaster*? *J. Comp. Physiol. A* **162**, 581-588.
Zanker, J. M. (1988b). On the mechanism of speed and altitude control in *Drosophila melanogaster*. *Physiol. Entomol.* **13**, 351-361.
Zanker, J. M., Egelhaaf, M. and Warzecha, A.-K. (1991). On the coordination of motor output during visual flight control of flies. *J. Comp. Physiol. A* **169**, 127-134.